Fluid-Elastic Waves between the Tectorial Membrane and the Organ of Corti

S.J. Elliott

ISVR Technical Memorandum No 952

October 2005

SCIENTIFIC PUBLICATIONS BY THE ISVR

Technical Reports are published to promote timely dissemination of research results by ISVR personnel. This medium permits more detailed presentation than is usually acceptable for scientific journals. Responsibility for both the content and any opinions expressed rests entirely with the author(s).

Technical Memoranda are produced to enable the early or preliminary release of information by ISVR personnel where such release is deemed to the appropriate. Information contained in these memoranda may be incomplete, or form part of a continuing programme; this should be borne in mind when using or quoting from these documents.

Contract Reports are produced to record the results of scientific work carried out for sponsors, under contract. The ISVR treats these reports as confidential to sponsors and does not make them available for general circulation. Individual sponsors may, however, authorize subsequent release of the material.

UNIVERSITY OF SOUTHAMPTON

INSTITUTE OF SOUND AND VIBRATION RESEARCH

SIGNAL PROCESSING & CONTROL GROUP

Fluid-Elastic Waves between the Tectorial Membrane and the Organ of Corti

by

S J Elliott

ISVR Technical Memorandum N° 952

October 2005

Authorised for issue by
Prof R Allen
Group Chairman

ACKNOWLEDGEMENT

CONTENTS

FIGURES

1. Introduction

It is important to understand the micromechanical behaviour of the organ of Corti because it is the site of the cochlear amplifier that provides us with our exquisite hearing sensitivity. A sketch of the major components of the organ of Corti is shown on the left hand side of Figure 1. Previous micromechanical models (e.g. Neely and Kim, 1986) have assumed that the basilar membrane (BM) and tectorial membrane (TM) behave individually as single degree of freedom systems, with an associated lumped mass and stiffness, connected together via a spring representing the stiffness of the outer hair cell stereocillia. Such a lumped parameter model is shown on the right hand side of Figure 1.

More recently Bell and Fletcher (2004) have suggested that the tectorial membrane and reticular lamina may have a bending stiffness that acts together with the fluid inertia in the subtectorial gap to generate wave motion in this small space, with a phase velocity that is slow enough that resonances can occur along the 80μm or so length of the subtectorial gap. In this report we examine another possible distributed model of the organ of Corti, in which the tectorial membrane is assumed to behave as a locally-reacting elastic body.

There is some evidence for this model from the mechanical measurements made on the tectorial membrane by Freeman et al. (2003) and the organ of Corti by Scherer and Gummer (2004). Freeman et al. used both magnetically-actuated beads and a force probe to measure the mechanical impedance of the surface of tectorial membranes from mice, when laid out on a solid surface. They concluded that the dynamic behaviour up to several kHz could be well represented as a lossy stiffness of about $0.2\ \mathrm{Nm^{-1}}$ in the transverse direction, when measured with a force probe of diameter of about 50 μm. The measured losses can be reasonably well represented by assuming a complex stiffness of the form

$$K = K_o(1 + j\mu) \tag{1.1}$$

where K_o is the magnitude of the mechanical stiffness and μ is a loss factor. This model predicts that the mechanical impedance will have a phase shift of $-\tan^{-1}\frac{1}{\mu}$. The transverse impedance measured by Freeman et al. (2003), has an almost frequency independent phase shift of about −60° from 10Hz to 4kHz, so that μ is predicted to be approximately constant, with a value of about 0.5.

Scherer and Gummer (2004) measured the mechanical impedance at various points along the upper surface of the organ of Corti, labelled the reticular lamina in Figure 1, using an atomic force cantilever, with a typical indentation depth of 1 μm. They measured impedances consistent with a lossy spring having a spring constant that fell from about 0.5 Nm^{-1} at the tunnel of Corti to about 0.05 Nm^{-1} at the outer tunnel, with the stiffness at the positions of the three outer hair cells falling in between these values. The damping they measured could also be modelled reasonably well with a complex stiffness of the form of equation (1.1) with a loss factor, μ, again having a value of about 0.5.

2. An Elastic Model

The behaviour of various models of an elastic surface is discussed, for example, by Johnson (1985). One widely-used model of an elastic surface is the Winkler bedding, in which the elastic behaviour of a surface is modelled by an array of linear springs of stiffness K_Δ, separated by a distance Δ, as shown for a rigidly-backed elastic layer in Figure 2. Provided the load is applied over an area which is large compared with Δ^2, then the exact spacing of the elemental springs does not affect the behaviour provided

$$K_\Delta \big/ \Delta^2 = \kappa, \tag{2.1}$$

which is the stiffness per unit area, is a constant. If the load is applied over a disc of radius a, the mechanical stiffness would thus be equal to

$$K = \pi a^2 \kappa. \tag{2.2}$$

The Winkler bedding model implicitly assumes that the deformation is local, so that there is no deflection at points away from where the load is applied, and that the deformation shape is also unaffected by the thickness of the elastic material.

As the thickness, T, of an elastic layer on a rigid surface becomes significant compared with the lengthscale of the load, a, then bulk effects in the material start to become important and alternative models must be used. In the extreme case where the thickness of the material is much larger than the lengthscale of the applied load, $T \gg a$ in Figure 2, then an elastic half-space model could be used. Johnson (1985) dates this model back to the work of Lamb in 1905, and shows (equation 11.11 p.346) that the dynamic stiffness experienced by a uniform circular load of radius a is equal to

$$K = Ga \left[h_1 + j \frac{\omega a}{c_2} h_2 \right],$$ (2.3)

where G is the elastic shear modulus, equal to $E/2(1-v)$ where E is the Young's modulus and v is Poisson's ratio, h_1 and h_2 are constants at a given frequency that are provided graphically by Johnson (1985), and c_2 is distortional wave velocity, which is of the order of 30 ms^{-1} for soft material like rubber.

This dynamic stiffness is equivalent to that of a linear spring in parallel with a viscous damper, for which the time constant is approximately equal to $0.7\, a/c_2$ for the values of h_1 and h_2 quoted by Johnson (1985). Assuming c_2 is about 30 ms^{-1}, this time constant is of the order of 200 ns for indentations with diameters of the order of 10 μm, so that this damping term can be ignored compared with that discussed in Section 1. Assuming that h_1 is about 5, from Figure 11.2 in Johnson, then the predicted mechanical stiffness in equation (2.3) is approximately

$$K = \frac{5Ea}{2(1-v)}.$$ (2.4)

Note that the stiffness is proportional to the indentation radius, a, rather than the indentation radius squared in the Winkler bedding model, equation (2.2). This difference can be rationalised by considering the stiffness of an equivalent cylinder of length T, which would be

$$K = \frac{\pi E a^2}{T}.$$

(2.5)

If T is small compared with a, then K is proportional to a^2 and the Winkler bedding model is appropriate. Comparing equation (2.5) with equation (2.2) also suggests that the stiffness per unit area, κ, for such an elastic layer is approximately equal to E/T. As the thickness of the material gets larger compared with a, and the strain distribution inside the material becomes concentrated around the indentation, then the effective value of T becomes proportional to a, and so K becomes proportional to a, as in the elastic half-space model.

Thus whether the elastic material is of thickness T and backed by a rigid surface, or forms an elastic half space, the displacement per unit force when a circular load of radius a is applied can be represented by the mechanical stiffness K, such that the ratio of the displacement, w, to the applied force, f, is

$$\frac{w}{f} = \frac{1}{K},$$

(2.6)

where $K = \kappa \pi a^2$ for the rigidly backed layer, with κ being the stiffness per unit area and $K = 5Ea/1(1-v)$ for an elastic half space. The quantity used, in Section 3, to derive the wave equation, however, is the displacement, w, per unit pressure, p, where the pressure is equal to $f/\pi a^2$ for a circular load of radius a. This quantity can be written as

$$\frac{w}{p} = \frac{1}{S},$$

(2.7)

where S is $K/\pi a^2$ and may be termed the wall stiffness. It is equal to κ for the rigidly-backed layer, and for the elastic half space is equal to

$$S = \frac{5E}{2\pi(1-\nu)a}.$$

(2.8)

A very similar result is obtained if instead of a circular force distribution, an infinite strip of width $2a$ is assumed (Johnson, p.348).

The other property noted by Johnson (p.50) is that, away from the concentrated load, the deflection pattern on the surface of an elastic half space falls off to zero as $1/r$, where r is the distance from the edge of the applied load. A more exact analysis is possible to take this local behaviour into account by decomposing the force and displacement fields into their wavenumber components. This local deflection behaviour is in contrast to the sharply delineated deflection pattern seen in Figure 2 for the Winkler bedding. In both cases, however, the surfaces may, to a reasonable approximation, be taken to be locally reacting.

This theory allows us to compute the effective Young's modulus of the tectorial membrane (TM) from the measurements of Freeman et al. (2003). The indentation of their force probe had a radius of about 25μm, which we could assume is small compared with the TM thickness in order to use the elastic half-space model. We can then predict the Young's modulus, from equation (2.4), to be

$$E \approx \frac{2K(1-\nu)}{5a},$$

(2.9)

where K is the measured stiffness, which is about 0.2 Nm^{-1} and the Poisson's radio, ν, for the gel-like TM may be taken as 0.5. The predicted value of the Young's modulus of the TM is thus about 1.6kPa. This is significantly smaller than the widely-used value of 30kPa quoted by Steele et al. (1995), although Bell (2005) reviews a number of studies which estimate the TM elasticity and reports a wide range of values that bracket the 1.6kPa value derived here.

A similar calculation could be performed using the measurements on the organ of Corti taken by Sherer and Gummer (2004), for which $K = 0.05$ Nm^{-1} to 0.5 Nm^{-1} and the indenter had a radius, a, of only about ½ µm. Assuming v is again about 0.5, the effective values of the Young's modulus calculated using equation (2.9) is now about 20 to 200 kPa. Although it can be argued that the organ of Corti does not behave like an elastic half-space, this calculation does suggest that the effective stiffness of the organ of Corti to a pressure loading, equation (2.7), is significantly greater than that of the tectorial membrane, and thus to a first approximation could be considered as being rigid.

It is perhaps misleading that the mechanical impedances measured for the tectorial membrane by Freeman et al. (2004) and organ of Corti by Sherer and Gummer (2003), respectively, have such similar values, since the size of the indenters used to take these two measurements was very different. It is clear from the discussion above that the measured stiffness of an elastic body is significantly affected by the size of the indenter used to take such measurements.

3. Fluid-Elastic Waves

We now consider the equation governing waves between an elastic layer, whose dynamics are modelled as a local stiffness, and a fluid-filled layer of thickness d above a rigid surface, as shown in Figure 3. All the variables are considered constant in the y direction so that only waves which propagate along the x direction are considered, although the fluid can flow in both the x and z direction.

Starting off in the time domain, we define the wall displacement at the surface of the elastic layer as being w and the fluid displacements in the x and z directions as being u and v. The fluid pressure is assumed to be p, which together with w are functions only of x, whereas u and v will depend on both x and z.

The fluid in the gap is assumed to be incompressible so that the conservation of its mass leads to the relationship between u and v;

$$\frac{\partial u}{\partial x} + \frac{\partial v}{\partial z} = 0.$$ (3.1)

The conservation of the fluid momentum, ignoring the effects of fluid viscosity for the time being, leads to the equation

$$\frac{\partial p}{\partial x} = -\rho \frac{\partial^2 u}{\partial t^2},$$ (3.2)

where ρ is the density of the fluid.

The fluid displacement in the z direction is now assumed to vary linearly across the thin fluid layer, so that it is zero at the rigid surface at $z = 0$ and equal to the displacement of the elastic wall, w, at $z = d$, so that

$$v = \frac{z}{d} w,$$ (3.3)

where w is only a function of x. The momentum of the fluid in the z direction can be ignored provided d is much smaller than the wavelength, which is equivalent to the "long-wave" approximation in cochlear macromechanical modelling (de Boer 1991).

Differentiating equation (3.3) with respect to z and using equation (3.1) we obtain

$$\frac{\partial u}{\partial x} = -\frac{w}{d}.$$ (3.4)

Differentiating equation (3.4) twice with respect to t then gives

$$\frac{\partial^3 u}{\partial x \partial t^2} = -\frac{1}{d} \frac{\partial^2 w}{\partial t^2},$$ (3.5)

which may be compared with the result obtained by differentiating equation (3.2) with respect of x;

$$\frac{\partial^3 u}{\partial x \partial t^2} = -\frac{1}{\rho}\frac{\partial^2 p}{\partial x^2},$$ (3.6)

to give

$$\frac{\partial^2 p}{\partial x^2} - \frac{\rho}{d}\frac{\partial^2 w}{\partial t^2} = 0.$$ (3.7)

We now use the properties of the elastic surface, which is assumed to react locally so that

$$w = \frac{1}{S}p,$$ (3.8)

where S is the wall stiffness, to give the final, second order, wave equation as

$$\frac{\partial^2 p}{\partial x^2} - \frac{\rho}{dS}\frac{\partial^2 p}{\partial t^2} = 0.$$ (3.9)

This can also be written as

$$\frac{\partial^2 p}{\partial x^2} - \frac{1}{c^2}\frac{\partial^2 p}{\partial t^2} = 0,$$ (3.10)

where the phase velocity is

$$c = \sqrt{\frac{dS}{\rho}}.$$ (3.11)

4. Calculation of the Phase Velocity

If the elastic surface acts like a rigidly-backed elastic layer, it is shown above that the wall stiffness, S, is equal to the constant stiffness per unit area κ, and so the phase velocity equals

$$c = \sqrt{\frac{d\kappa}{\rho}}.$$ (4.1)

This is frequency-independent and so the waves generated between a fluid gap and a rigidly-backed elastic layer are nondispersive, provided the wavelength is large compared with the thickness of the elastic layer.

Despite the apparent simplicity of equation (3.11), it is made more complicated for the elastic half-space model by the fact that the stiffness, S, given, from Section 2, as

$$S = \frac{SE}{2\pi(1-\nu)a},$$ (4.2)

is a function of the assumed radius of the load acting on the elastic surface, a, which must be related to the wavelength of the sinusoidal pressure distribution set up by the wave, λ.

In fact an exact analysis of the static displacement distribution in an elastic half-space subject to a one dimensional sinusoidal pressure distribution has also been presented by Johnson (1985, p.398), who shows that the displacement has the same corrugated distribution as the pressure and that the pressure per unit displacement is then given by

$$S = \frac{\pi E}{(1-\nu^2)\lambda}.$$ (4.3)

Setting equation (4.2) equal to equation (4.3) allows an effective lengthscale to be calculated as

$$a = \frac{5(1-\nu^2)}{2\pi^2(1-\nu)}\lambda .$$

(4.4)

Assuming that ν is equal to 0.5 the effective lengthscale, a, is thus about 0.38λ.

Substituting (4.3) into the square of the equation for the phase velocity, (3.11) gives

$$c^2 = \frac{\pi E d}{(1-\nu^2)\lambda\rho} .$$

(4.5)

Since λ is c/f or $2\pi c/\omega$, we can thus derive an expression for the phase velocity as

$$c = \left(\frac{E\omega d}{2(1-\nu^2)\rho} \right)^{\frac{1}{3}} .$$

(4.6)

The waves generated between a fluid gap and an elastic half-space are thus dispersive, with a speed which increases with frequency according to $\omega^{\frac{1}{3}}$.

If, for example, we assume that E is 1.6 kPa, d is 3μm, $f = \omega/2\pi$ is 1 kHz, ρ is 1000 kgm^{-3} and $\nu = 0.5$, then the predicted phase velocity is about 270 mms^{-1}, and the wavelength is about 270μm.

5.   The Effect of Fluid Viscosity and Elastic Damping

For the small fluid gaps important in cochlear micromechanics the viscosity of the fluid will play a significant role in the dynamic behaviour. The measurements of the tectorial membrane dynamics by Freeman et al. (2003) also showed that the local stiffness has a significant loss, with a loss factor of about 0.5. Both of these effects

will cause a propagating wave to decay, but will also modify the phase velocity, and so it is important to take them into account.

The fluid viscosity will give rise to an additional term in equation (3.2) due to drag, whose magnitude will depend on the relative values of the fluid gap thickness, d, and the viscous boundary layer thickness given by

$$\delta = \left(\frac{\eta}{\rho\omega}\right)^{\frac{1}{2}}, \tag{5.1}$$

where η is the coefficient of viscosity, which is approximately $7\times10^{-4}\,\mathrm{kg\ m^{-1}s^{-1}}$ for water at body temperature. The viscous boundary layer thickness is thus about $10\mu m$ at a frequency of 1 kHz and is somewhat larger than the fluid gap thickness, which is of the order of $3\mu m$. The flow in the x direction will thus approximate the parabolic profile of Poiseuille and the force required to overcome viscosity will be approximately $\left(4\eta/d^2\right)\partial u/\partial t$ (Lamb, 1925). The fluid force equation, (3.2), with viscosity then becomes

$$\frac{\partial p}{\partial x} = -\rho\frac{\partial^2 u}{\partial t^2} - \frac{4\eta}{d^2}\frac{\partial u}{\partial t}. \tag{5.2}$$

Thus

$$\frac{\partial^2 u}{\partial t^2} = -\frac{1}{\rho}\frac{\partial p}{\partial x} - \frac{4\eta}{\rho d^2}\frac{\partial u}{\partial t}, \tag{5.3}$$

and so

$$\frac{\partial^3 u}{\partial t^2 \partial x} = -\frac{1}{\rho}\frac{\partial^2 p}{\partial x^2} - \frac{4\eta}{\rho d^2}\frac{\partial^2 u}{\partial x\partial t}. \tag{5.4}$$

But from equation (3.4), we know that

$$\frac{\partial u}{\partial x} = -\frac{w}{d} \tag{5.5}$$

so that

$$\frac{\partial^3 u}{\partial t^2 \partial x} = -\frac{1}{\rho}\frac{\partial^2 p}{\partial x^2} + \frac{4\eta}{\rho d^3}\frac{\partial w}{\partial t} = -\frac{1}{d}\frac{\partial^2 w}{\partial t^2}. \tag{5.6}$$

Thus equation (3.7) is modified by the effect of viscosity to become

$$\frac{\partial^2 p}{\partial x^2} - \frac{4\eta}{d^3}\frac{\partial w}{\partial t} - \frac{\rho}{d}\frac{\partial^2 w}{\partial t^2} = 0. \tag{5.7}$$

Assuming sinusoidal variations of the form $p(x)e^{j(\omega t - kx)}$ and $w(x)e^{j(\omega t - kx)}$, where $p(x)$ and $w(x)$ are the complex pressures and wall displacements at the angular frequency ω, equation (5.7) becomes

$$-k^2 p(x) - \frac{j\omega 4\eta}{d^3} w(x) + \frac{\omega^2 \rho}{d} w(x) = 0. \tag{5.8}$$

We now use the lossy version of the wall stiffness defined in equation (2.7) to relate the complex wall displacement to the complex pressure;

$$w(x) = \frac{1}{S(1+j\mu)} p(x) \tag{5.9}$$

so that the wave equation in the frequency domain becomes

$$-k^2 p(x) - \frac{j4\omega\eta}{d^3 S(1+j\mu)} p(x) + \frac{\omega^2 \rho}{d\,S(1+j\mu)} p(x) = 0. \tag{5.10}$$

The square of the wavenumber is thus given by

$$k^2 = \frac{\omega^2 \rho}{d \, S(1 + j\mu)} - \frac{j4\omega\eta}{d^3 S(1 + j\mu)} . \qquad (5.11)$$

Making the further assumption that the stiffness is that of an elastic half space, given by equation (4.3), with λ equal to $2\pi/\mathrm{Re}(k)$, where $\mathrm{Re}(k)$ is the real part of k, then

$$S = \frac{E \, \mathrm{Re}(k)}{2(1 - v^2)} . \qquad (5.12)$$

The wavenumbers are thus the solutions to the equation

$$k^2 \, \mathrm{Re}(k) = \frac{2\omega^2 \rho (1 - v^2)}{d \, E(1 + j\mu)} - \frac{j8\omega\eta (1 - v^2)}{d^3 \, E(1 + j\mu)} . \qquad (5.13)$$

If we set $k = \beta - j\alpha$, where β corresponds to the propagating part of the wavenumber and α to the attenuation constant, and we assume that the complex term on the right hand side of equation (5.13) is $R + jX$, then this equation can be written as

$$(\beta - j\alpha)^2 \, \beta = R + jX . \qquad (5.14)$$

Equating the real and imaginary parts of equation (5.14) leads to the simultaneous equations

$$\beta^3 - \alpha^2 \beta = R \quad \text{and} \quad 2\alpha \beta^2 = -X . \qquad (5.15,16)$$

Thus, for equation 5.16,

$$\alpha = -\frac{X}{2\beta^2} \qquad (5.17)$$

and substituting this into equation (5.15) leads to a quadratic equation in β^3

$$\beta^6 - R\,\beta^3 - \frac{X^2}{4} = 0, \qquad\qquad (5.18)$$

which can be solved for β, and hence α found using equation (5.17). The two valid solutions to these equations $k = \pm(\beta - j\alpha)$ correspond to waves propagating and decaying in the two directions.

Figure 4 shows the way that the phase speed, ω/β, and attenuation coefficient, α, vary as a function of frequency when we assume that $E = 1.6\mathrm{kPa}$, d is $3\mu\mathrm{m}$, $\rho = 1000\mathrm{kgm}^3$ and $v = 0.5$. Four graphs are shown, for the lossless case, $\eta = 0$, $\mu = 0$, dotted; for loss only in the elastic half space, $\eta = 0$, $\mu = 0.5$ dot-dashed; for loss only in the fluid, $\eta = 6.6 \times 10^{-4}\mathrm{PaS}$, $\mu = 0$ light solid; and for loss in both the elastic half space and the fluid, $\eta = 6.6 \times 10^{-4}\mathrm{PaS}$, $\mu = 0.5$ thick solid.

It can be seen that the losses in the elastic half space introduce some attenuation and a slight increase in the phase speed, whereas the fluid viscosity in this geometry leads to significant attenuation and lowers the phase speed by about a factor of three. The phase speed at 1kHz taking both effects into account is about $100\mathrm{mms}^{-1}$, so that the wavelength is about $100\mu\mathrm{m}$. The overall attenuation coefficient at 1kHz, however, is about $100\mathrm{mm}^{-1}$, so that the wave decays by a factor of $\frac{1}{e}$ over a length scale of about $10\mu\mathrm{m}$. With this assumed geometry the fluid elastic wave is thus very heavily damped.

6.   Conclusions

A model of the micromechanical dynamics of the organ of Corti has been considered in which the tectorial membrane is considered as an elastic half space and the fluid in the subtectorial space is incompressible. A simple model of an elastic half space is used to deduce a value for the Young's modulus of the tectorial membrane from the mechanical impedance measurements reported by Freeman et al. (2003), which at

about 1.6kPa is somewhat lower than the value generally assumed in previous models. The measured losses could be accounted for by assuming a simple form for the complex stiffness.

The upper surface of the organ of Corti is assumed to be rigid to a first approximation. A phenomenological model is then used to derive an equation describing the fluid-elastic waves that are predicted to propagate in this simplified mechanical system, which have a lossless phase velocity proportional to $\omega^{\frac{1}{3}}$. The waves are slowed as well as attenuated by the viscosity of the fluid, which appears to be more important than the losses in the elastic half space for the geometry assumed here.

For this geometry the wave is very heavily attenuated over its wavelength and no resonant behaviour would be expected for the passive system. It is still possible, however, that the active behaviour of the outer hair cells could overcome these losses by amplifying the response at certain frequencies, as observed for the fluid-bending stiffness waves of Bell and Fletcher (2004) by Elliott et al. (2005).
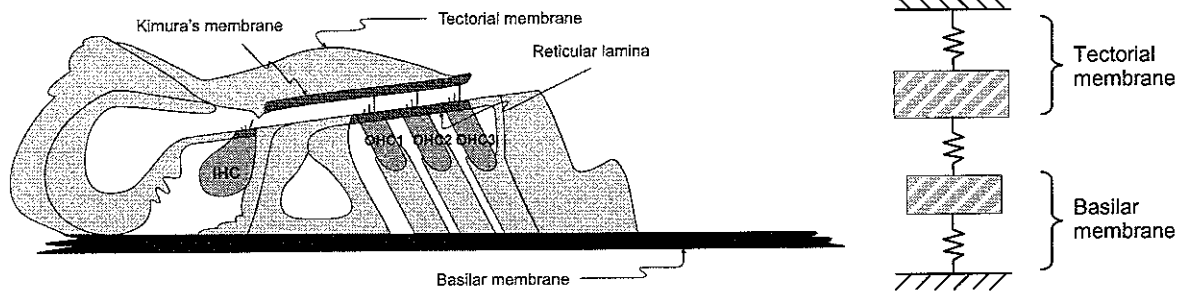
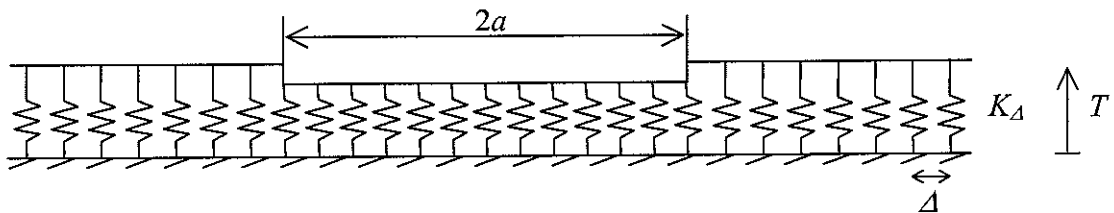Figure 1. Diagram of the organ of Corti, left, and its lumped parameter model, right.

Figure 2. Cross-section of Winkler bedding model of the elastic behaviour of an elastic material on a rigid surface with an external pressure applied over a disc of radius a.
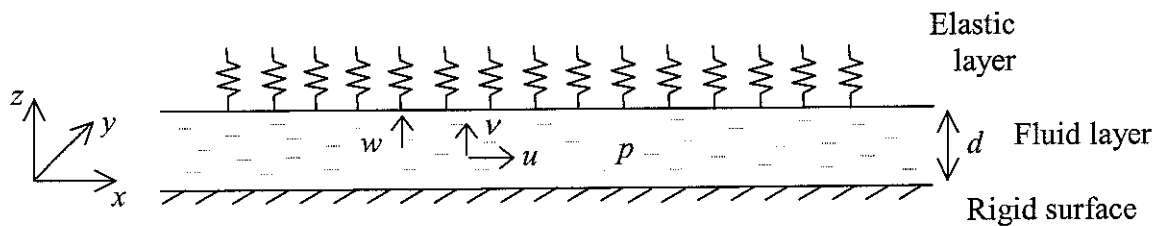

Figure 3. Geometry of the fluid layer, in which the longitudinal and transverse fluid displacements are u and v and the pressure is p, between a rigid surface and an elastic layer in which the transverse displacement is w.

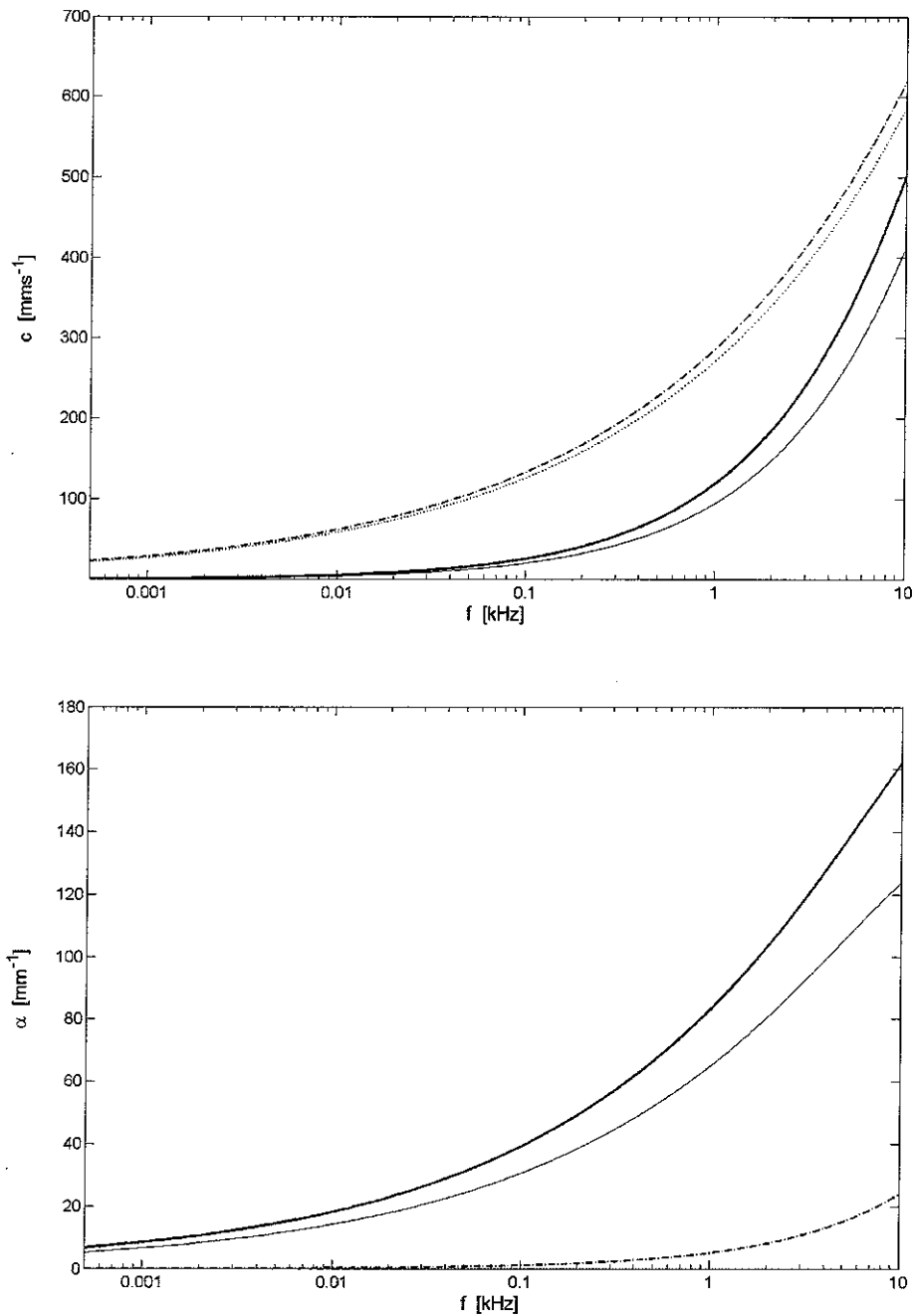Figure 4. The phase speed, c, (upper) and attenuation coefficient, α, (lower) calculated for a fluid-elastic wave in the subtectorial space with no losses ($\eta = 0$, $\mu = 0$), dotted, with loss only in the elastic half space ($\eta = 0$, $\mu = 0.5$); dot-dashed losses in only the fluid ($\eta = 6.6 \times 10^{-4}$, $\mu = 0$); feint solid, and losses in both the elastic half space and fluid ($\eta = 6.6 \times 10^{-4}$ PaS, $\mu = 0.5$); thick solid.

References

S.T.Neely and D.O.Kim, "A model for active elements in cochlear biomechanics", *J. Acoust. Soc. Am.*, **79**(5), 1472-1480 (1986).

A.Bell and N.H.Fletcher, "The cochlear amplifier as a standing wave: "Squirting" waves between rows of outer hair cells?", *J. Acoust. Soc. Am.*, 116(2), 1016-1024 (2004).

D.M.Freeman, C.Cameron Abnet, W.Hemmert, B.S.Tsai and T.F.Weiss, "Dynamic material properties of the tectorial membrane: a summary", *Hearing Research*, **180**, 1-10 (2003).

M.P.Scherer and A.W.Gummer, "Impedance analysis of the organ of Corti with magnetically actuated probes", *Biophysical Journal*, 87, 1378-1391 (2004).

K.L.Johnson, *Contact Mechanics*, Cambridge University Press (1985).

R.Steel, G.J.Baker, J.A.Tolomeo and D.E.Zetes, "Cochlear mechanics" in *Biomedical Engineering Handbook*, IEEE Press Series (1995).

H.Lamb, *The Dynamical Theory of Sound*, reprinted in Dover edition 1960 (1925).

J.A.Bell, *The Underwater Piano: A Resonance Theory of Cochlear Mechanics,* PhD Thesis, The Australian National University, Canberra (2005).

S.J.Elliott, R.Pierzycki and B.Lineton, "Incorporation of an active feedback loop into the squirting wave model of the cochlear amplifier", *Proc. Int. Conf. Sound and Vibration (ICSV12)*, Lisbon (2005).